On the role of subgrid-scale coherent modes in large-eddy simulation

By G. DE STEFANO[1], D. E. GOLDSTEIN[2]
AND O. V. VASILYEV[2]†

[1]Dipartimento di Ingegneria Aerospaziale e Meccanica, Seconda Universitá di Napoli,
I 81031 Aversa, Italy

[2]Department of Mechanical Engineering, University of Colorado, 427 UCB, CO 80309 Boulder, USA

The role of coherent and incoherent subgrid-scale modes in large-eddy simulation modelling is examined. The coherent/incoherent decomposition of the subgrid-scale stresses based on the wavelet de-noising procedure is introduced. *A priori* dynamical tests based on the *perfect* modelling approach are performed for decaying isotropic turbulence. The theoretical effects of coherent and incoherent subgrid-scale forces are dynamically evaluated during the simulation. The relation between deterministic/ stochastic subgrid-scale models and coherent/incoherent subgrid-scale stresses is discussed. The main result is that in large-eddy simulations low-order statistics can be almost exactly reproduced when only the effect of the coherent subgrid-scale modes is accounted for, while the incoherent subgrid-scale modes have a negligible effect upon the large-scale dynamics and the energy transfer.

1. Introduction

In large-eddy simulation (LES) of turbulent flow, the formal scale separation is obtained by means of a low-pass filtering operation applied to the Navier–Stokes equations, which leads to the definition of filtered (or large-scale) and residual (or small-scale) fields. The filtered Navier–Stokes equations must be closed by modelling the subgrid-scale (SGS) stresses that account for the effect of the unresolved small-scale eddies. The nearly universal approach in LES is to use deterministic models, where the SGS stresses are defined as a given function of the large-scale (resolved) velocity field (e.g. Smagorinsky 1963; Bardina, Ferziger & Reynolds 1983; Germano *et al.* 1991; Lesieur & Métais 1996; Meneveau & Katz 2000).

An alternative approach is to use stochastic modelling by also considering a noise contribution to the SGS model. For instance, a stochastic force can be added to a classical eddy viscosity term to develop improved SGS models (e.g. Chasnov 1991). The motivation behind stochastic modelling is the recognition that the large scales of motion are randomly forced through nonlinear interaction with small-scale eddies resulting in stochastic backscatter of energy (e.g. Leith 1990). Stochastic models more realistically mimic the behaviour of filtered direct numerical simulation (DNS), since different flow realizations are observed for the same initial large-scale field. However, the flow realizations for stochastic LES are different from the filtered DNS solution. In fact, it is impossible to construct an LES model providing large-scale velocity that matches the filtered DNS field realization by realization. To achieve statistical

† Author to whom correspondence should be addressed.

correspondence between the LES and DNS fields, Langford & Moser (1999) considered an optimal LES formulation, where the SGS force is characterized by a statistical distribution that is modelled via a stochastic estimation technique (Adrian 1990). It has been found that the error between the real and estimated SGS force is as large as the SGS force itself. However, despite the large error, the optimal LES model exactly represents the total energy transfer to the subgrid scales.

To understand the effect of deterministic versus stochastic modelling in LES one must go back to the basic structures of turbulence. Turbulence is characterized by energetic eddies that are localized in space and contain significant energy at all length scales, from the characteristic length scale of the physical domain down to the Kolmogorov length scale (e.g. Jimenez *et al.* 1993; Farge, Pellegrino & Schneider 2001; Goldstein & Vasilyev 2004). Visual studies of turbulent velocity fields have shown the presence of basic three-dimensional structures, namely vorticity tubes, often referred to as wormlike structures, at all the scales of the flow (Vincent & Meneguzzi 1991). Thus, when a low-pass filter is used with LES, the small-scale coherent energetic eddies are filtered out. Therefore, the effect of these small-scale coherent energetic structures contained in the subgrid scales, hereafter referred to as the coherent SGS modes, must be modelled. It has been hypothesized from preliminary results in Goldstein & Vasilyev (2004) that the coherent SGS modes have a disproportionately large effect on the total SGS dissipation and, consequently, on the evolution of the resolved LES field.

While numerous previous publications have dealt with the role of coherent energetic eddies in the context of DNS, coherent vortex simulation (CVS) (e.g. Farge, Schneider & Kevlahan 1999) and stochastic coherent adaptive LES (SCALES) (e.g. Goldstein & Vasilyev 2004) or with the role of 'near-band' SGS modes (e.g. Kraichnan 1976; Domaradzki, Liu & Brachet 1993; Domaradzki *et al.* 1994), the main objective of the present work is to rigorously study the effect of the coherent/incoherent SGS modes on the evolution of the resolved modes in the classical LES approach. The coherent/incoherent turbulence decomposition is based on wavelet de-noising. In particular, we adopt the simple idea, originally introduced by Farge *et al.* (1999), according to which the coherent eddies correspond to the de-noised flow field, which is very different from other known definitions (e.g. Cantwell 1981; Hussain 1986; Lesieur 1997). The de-noising procedure is conducted through wavelet filtering, that is performed in wavelet space by wavelet coefficient thresholding. Previous studies have clearly demonstrated that, for a suitable thresholding level, such a filter is able to decompose an instantaneous turbulent field into a non-Gaussian coherent part (corresponding to the energetic coherent eddies) and an incoherent one, which is close to Gaussian white noise (Farge *et al.* 1999, 2001; Goldstein & Vasilyev 2004).

The present analysis is conducted for isotropic turbulence, by means of the *perfect* modelling procedure, an *a priori* dynamical test originally introduced by De Stefano & Vasilyev (2002, 2004). It will be shown in this paper that in LES a small number of coherent SGS modes, which contain the majority of the SGS energy, are also responsible for the clear majority of the SGS dissipation, while the incoherent modes, that account for the majority of the SGS modes, contribute a negligible amount to the total SGS dissipation. Due to the drastically different global effects of the coherent and incoherent SGS modes upon the large-scale dynamics, one can argue that different SGS models can and should be adopted for the corresponding contributions to the LES solution. Namely, deterministic models must be used to mimic the effect of the unresolved coherent modes and stochastic models for the incoherent ones.

Note that the present study should be distinguished from earlier publications (e.g. Kraichnan 1976; Domaradzki *et al.* 1993, 1994) that studied the contribution of

'near-band' SGS modes, namely those not smaller than about half of the smallest resolved scales, and concluded that the SGS dissipation results almost exclusively from the interactions between resolved scales and 'near-band' modes. The main distinction is that 'near-band' modes contain both coherent and incoherent SGS modes. In order to make this distinction clear, we also explicitly compare the dynamical effect of these 'near-band' SGS stresses to that of the coherent SGS stresses.

The rest of the paper is organized as follows. In §2, the entire methodology is presented. In particular, in §2.1 some wavelet properties are discussed, while the wavelet de-noising theory is introduced in §2.2. The concept of coherent/incoherent decomposition based on wavelet de-noising is briefly discussed in §2.3 and the consistent definition of coherent and incoherent SGS stresses is introduced in §2.4. The *perfect* modelling procedure is briefly reviewed in §2.5. In §3 results of numerical experiments are presented and the role of coherent modes in SGS modelling is shown. Finally, in §4 conclusions are drawn.

2. Methodology

2.1. *Wavelet properties*

Wavelets are basis functions which are localized in both physical (due to their finite support) and wavenumber space. For comparison, the classical Fourier transform is based on functions (sines and cosines) that are well-localized in frequency but do not provide localization in physical space (due to their global support). Because of this space/scale localization, the wavelet transform provides both spatial and scale (frequency) information, while the Fourier transform on the other hand only provides frequency information.

A field $u(x)$ can be represented in terms of wavelet basis functions as

$$u(\boldsymbol{x}) = \sum_{\boldsymbol{l} \in \mathscr{L}^0} c_{\boldsymbol{l}}^0 \phi_{\boldsymbol{l}}^0(\boldsymbol{x}) + \sum_{j=0}^{+\infty} \sum_{\mu} \sum_{\boldsymbol{k} \in \mathscr{K}^{\mu,j}} d_{\boldsymbol{k}}^{\mu,j} \psi_{\boldsymbol{k}}^{\mu,j}(\boldsymbol{x}), \tag{2.1}$$

where $\phi_{\boldsymbol{k}}^0(\boldsymbol{x})$ and $\psi_{\boldsymbol{l}}^{\mu,j}$ are n-dimensional scaling functions and wavelets of different families (μ) and levels of resolution (j), respectively (e.g. Vasilyev 2003). Scaling function coefficients represent the averaged values of the field, while the wavelet coefficients represent the details of the field at different scales. The wavelet functions have a zero mean, while the scaling functions do not.

Traditionally, wavelets ψ_k^j are constructed by the discrete (typically dyadic) dilation and translation of a single mother wavelet $\psi(x)$, i.e. $\psi_k^j(x) = \psi(2^j x - k)$. This results in the construction of the first-generation wavelets (e.g. Daubechies 1988) that are defined either in infinite or periodic domains. The second-generation wavelets (Sweldens 1998) are a generalization of first-generation wavelets that supplies the necessary freedom to deal with complex geometries, arbitrary boundary conditions, and irregular sampling intervals. Second-generation wavelets form a Reisz basis for $\mathbf{L}_2$ space, with the wavelets often having many vanishing polynomial moments, but without the translation and dilation invariance of their first-generation cousins. Despite the loss of this fundamental property of wavelet bases, second-generation wavelets retain many of the useful features of first-generation ones, including a fast $O(N)$ transform. The construction of second-generation wavelets is based on the lifting scheme that is discussed in detail by Sweldens (1998).

For this study we use a set of second-generation wavelets known in the literature as lifted interpolating wavelets. For a deeper discussion on the construction of

second-generation wavelets the reader is referred to the paper by Sweldens (1998). For a more general discussion on wavelets we refer to the book by Mallat (1999).

2.2. *Wavelet de-noising*

The wavelet de-noising procedure, also called wavelet shrinkage, was originally introduced by Donoho (1994). It can be briefly described as follows: given a function that is the superposition of a smooth function and noise, one performs a forward wavelet transform, and sets to zero the 'noisy' wavelet coefficients if the square of the wavelet coefficient is less than the noise variance. This procedure, known as hard or linear thresholding, is optimal for de-noising signals in the presence of Gaussian white noise, since wavelet-based estimators minimize the maximal L_2-error for functions with inhomogeneous regularity.

The wavelet de-noising procedure can be formally written by taking wavelet decomposition (2.1) and setting to zero wavelet coefficients that are below a given threshold, ϵ. This procedure results in the following de-noised field:

$$u_>(\boldsymbol{x}) = \sum_{\boldsymbol{l} \in \mathscr{L}^0} c_{\boldsymbol{l}}^0 \phi_{\boldsymbol{l}}^0(\boldsymbol{x}) + \sum_{j=0}^{+\infty} \sum_{\mu} \sum_{\substack{\boldsymbol{k} \in \mathscr{K}^{\mu,j} \\ |d_{\boldsymbol{k}}^{\mu,j}| > \epsilon}} d_{\boldsymbol{k}}^{\mu,j} \psi_{\boldsymbol{k}}^{\mu,j}(\boldsymbol{x}). \tag{2.2}$$

It is worth stressing that the wavelet thresholding filter is a nonlinear filter that depends on each flow realization.

2.3. *Coherent/incoherent decomposition*

It has been demonstrated previously (Farge *et al.* 1999, 2001; Goldstein & Vasilyev 2004) that when a wavelet thresholding filter is applied to an isotropic turbulence velocity or vorticity field, by using the correct thresholding level ϵ, the turbulent field is decomposed into coherent (organized), $u_>$, and incoherent (nearly Gaussian white noise), $u_<$, fields:

$$u = u_> + u_<. \tag{2.3}$$

Then, by construction, the coherent field can be defined as the wavelet-filtered field as it contains the coherent energetic structures that were not removed by the wavelet filtering (or de-noising) operation. Wavelet compression will be defined as $(N - N_>)/N$, where N is the total number of wavelet coefficients and $N_>$ is the number of retained wavelet coefficients after wavelet thresholding. In this work we are interested in the coherent and incoherent modes in the SGS velocity field and how they interact with the LES solution. Note that the wavelet filtering operation does not conserve divergence. For incompressible flow, in order to ensure that the wavelet-filtered (coherent) field is divergence-free, an additional divergence-free projection operation is performed after the wavelet filtering operation.

2.4. *SGS stresses decomposition*

Consider the filtered incompressible Navier–Stokes equations,

$$\frac{\partial \overline{u}_j}{\partial t} + \frac{\partial \overline{u_j u_k}}{\partial x_k} = -\frac{1}{\rho} \frac{\partial \overline{p}}{\partial x_j} + \nu \frac{\partial^2 \overline{u}_j}{\partial x_k \partial x_k} - \frac{\partial \overline{\tau}_{jk}}{\partial x_k}, \tag{2.4}$$

where filtered quantities are denoted with a bar. Here, owing to the adoption of a pseudo-spectral method for the numerical experiments, a sharp cutoff filter is assumed. This way, the separation between resolved and unresolved scales is unambiguous and the small-scale field, $u_j' \equiv u_j - \overline{u}_j$, does not contain resolved wavenumber components.

In (2.4) the SGS stresses are defined as

$$\overline{\tau}_{jk} = \overline{u_j u_k} - \overline{\overline{u}_j \overline{u}_k} \tag{2.5}$$

or, equivalently, in terms of the small-scale field, $\overline{\tau}_{jk} = \overline{\overline{u}_j u'_k} + \overline{u'_j \overline{u}_k} + \overline{u'_j u'_k}$. Once the SGS field has been decomposed into coherent $u'_{j>}$ and incoherent $u'_{j<}$ parts, $u'_j = u'_{j>} + u'_{j<}$, the SGS stresses can be consistently split. In fact, the effect of SGS coherent modes is due to large-scale/coherent SGS as well as to coherent/coherent SGS interaction and is taken into account by the following stresses, hereafter referred to as *coherent* SGS stresses:

$$\overline{\tau}_{jk}^{(\text{coh})} = \overline{\overline{u}_j u'_{k>}} + \overline{u'_{j>} \overline{u}_k} + \overline{u'_{j>} u'_{k>}}. \tag{2.6}$$

Note that, despite the name, these stresses do not correspond to wavelet-filtered SGS stresses, $\overline{\tau}_{jk>}$.

Analogously, the effect of large-scale/incoherent SGS, coherent/incoherent and incoherent/incoherent subgrid-scale interactions is taken into account by the *incoherent* SGS stresses,

$$\overline{\tau}_{jk}^{(\text{inc})} = \overline{\overline{u}_j u'_{k<}} + \overline{u'_{j<} \overline{u}_k} + \overline{u'_{j>} u'_{k<}} + \overline{u'_{j<} u'_{k>}} + \overline{u'_{j<} u'_{k<}}. \tag{2.7}$$

This way, the SGS stresses split according to

$$\overline{\tau}_{jk} = \overline{\tau}_{jk}^{(\text{coh})} + \overline{\tau}_{jk}^{(\text{inc})} \tag{2.8}$$

and the same decomposition holds for the SGS dissipation, $\epsilon_{SGS} \equiv -\langle \overline{\tau}_{jk} \overline{S}_{jk} \rangle$, where the $\overline{S}_{jk}$ are the components of the large-scale velocity strain-rate tensor and $\langle \cdot \rangle$ denotes ensemble averaging. In fact, the separate contributions from coherent and incoherent SGS fields can be defined as *coherent* SGS dissipation, $\epsilon_{SGS}^{(\text{coh})} \equiv -\langle \overline{\tau}_{jk}^{(\text{coh})} \overline{S}_{jk} \rangle$, and *incoherent* SGS dissipation, $\epsilon_{SGS}^{(\text{inc})} \equiv -\langle \overline{\tau}_{jk}^{(\text{inc})} \overline{S}_{jk} \rangle$.

In a real LES the SGS stresses are unknown quantities, which must be somehow modelled in terms of the resolved field. In this analysis, the effect of coherent and incoherent SGS stresses is considered using the perfect modelling approach, which is briefly discussed next.

2.5. *Perfect modelling approach*

In order to avoid misunderstanding, it is first stressed that the perfect modelling procedure is not an SGS model. It consists of supplying LES with the ideal SGS stresses evaluated by definition from the reference DNS solution (De Stefano & Vasilyev 2004). Namely, by conducting a preliminary spectral DNS, a wavelet filter is applied to the DNS velocity field to decompose it into energetic coherent modes and incoherent background noise, according to the de-noising procedure discussed in §2.2. Also, a sharp cutoff filter corresponding to the LES grid is applied to both coherent and incoherent fields to separate large- from small-scale motions. The procedure is repeated at each time step so that both the coherent and incoherent SGS stresses are evaluated using (2.6) and (2.7) and the SGS forces are stored on the space–time LES grid. Note that, when applying the wavelet filter, given the desired compression, the effective threshold ϵ should change in time with the solution. However, it has been verified that it does not vary much and, thus, it has been kept constant in the following experiments.

The study is conducted by performing three different simulations, namely LES supplied with: only the perfect coherent stresses (denoted C – LES), only the perfect incoherent stresses (I – LES), and the perfect total stresses (T – LES). In order to make a comparison with known results from *a priori* studies on local/distant SGS
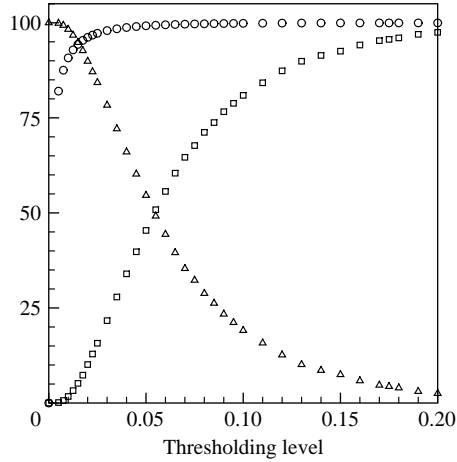
FIGURE 1. Percent fraction of 'coherent' (△) and 'incoherent' (□) SGS dissipation together with the compression (○) versus the wavelet thresholding level for LES with $\kappa_c = 16$.

interactions, an additional LES supplied with the SGS stresses from the 'near-band' modes, namely those for which $\kappa_c < \kappa < 2\kappa_c$, has been performed (B – LES), where κ_c is the LES cutoff wavenumber.

3. Numerical experiments

3.1. *Simulation settings*

Decaying isotropic turbulence is considered as the flow model for the numerical experiments. The initial Reynolds number of the flow is fixed at a moderate value, i.e. $Re_\lambda = 72$, λ being the Taylor microscale. The same classical pseudo-spectral code with full de-aliasing is used for both the reference DNS and the LES solutions. The DNS is performed on a 128^3 grid (a 192^3 grid is used for full de-aliasing of nonlinear terms according the 3/2 rule). The time integration step is set at about 10^{-3} times the initial eddy-turnover time. The initial conditions are obtained by random forcing of the flow field using the scheme proposed by Eswaran & Pope (1988), until an equilibrium stationary state has been reached and the inertial range has developed to some extent. The time integration is stopped after 10^3 time steps, i.e. when the energy content of the flow has become almost half the initial value. Two different LES grids are considered, 16^3 and 32^3 with the cutoff wavenumber adopted for large/small-scale decomposition being fixed at $\kappa_c = 8$ and 16, respectively.

As far as wavelet filtering is concerned, the choice of the wavelet thresholding level ϵ is crucial. Figure 1 shows the compression and the percent fraction of the SGS dissipation due to 'coherent' and 'incoherent' SGS stresses, as a function of ϵ, for the initial velocity field (32^3 LES case). Note that we used the terms 'coherent' and 'incoherent' in inverted commas to emphasize that, for varying thresholding level, it is better to think about SGS dissipation induced by wavelet-filtered and residual SGS modes instead. Also note that for a given turbulent velocity field there is an optimal value of ϵ for which the wavelet filter decomposes the velocity field into a filtered field that contains all the coherent vortices of significant energy and a residual field that is as close to Gaussian white noise as possible (Goldstein & Vasilyev 2004). This optimal value minimizes the $\mathbf{L}_\infty$-error between the probability density function (PDF) of the residual field and a Gaussian PDF with the same mean and variance. Another
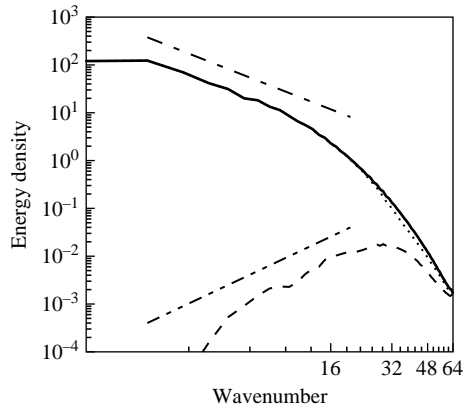
FIGURE 2. Energy spectra for full (——), coherent (········) and incoherent (– – –) DNS fields. The ideal slopes $-5/3$ (— · —) for the inertial range and 2 (— · · —) for energy equipartition are also shown.
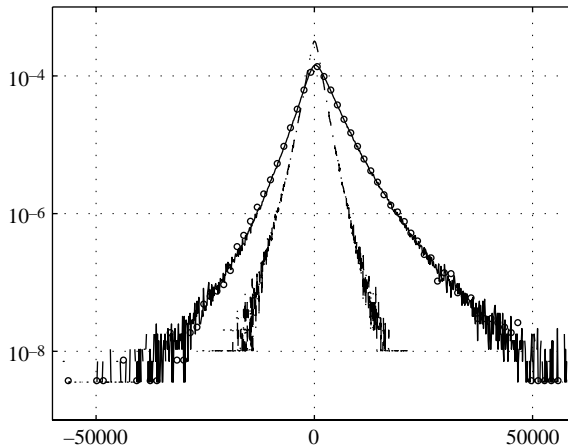

FIGURE 3. PDF of 'coherent' (——), 'incoherent' (— · —) and total (○) SGS dissipation for the initial field.

way to define the optimal wavelet coefficients thresholding level is to base it on the SGS dissipation. As the SGS dissipation does not have a minimum (see figure 1), an additional constraint must be added in order to maximize the field compression at the same time. Based on this combined criterion the optimal wavelet threshold can be defined, resulting in $\epsilon = 1.5 \times 10^{-2}$ for the case considered, that is a time-average field compression of 94%. It has been verified that the residual incoherent field corresponds to a nearly Gaussian white noise. In fact, as illustrated in figure 2, the shell energy spectrum for the incoherent DNS velocity has a κ^2-slope in the inertial range, that corresponds to energy equipartition in wavenumber space.

Finally, it is worth stressing that in our simulations significant backscatter is present from both coherent and incoherent SGS modes. This issue is clarified in figure 3, where the PDF of coherent, incoherent and total SGS dissipation is reported. The coherent SGS dissipation has almost the same PDF as the full one showing a positive mean, corresponding to a net energy transfer from large to small scales. On the
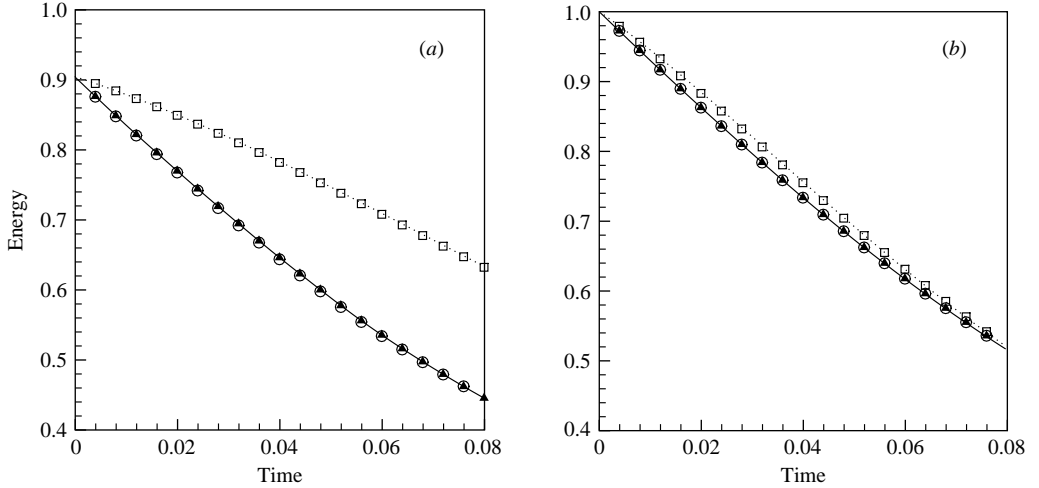
FIGURE 4. Energy decay for C – LES (▲), I – LES (□), and B – LES (○) compared to truncated DNS (———) and no-modelled solutions (·······) with (a) $\kappa_c = 8$ and (b) 16.

contrary, the PDF of the incoherent SGS dissipation is characterized by a nearly zero mean and a significantly lower variance. Note that, while the incoherent background noise does not contribute globally to the SGS dissipation, the incoherent SGS modes cause local bi-directional energy transfer with the resolved modes, as it clearly appears from the figure.

3.2. *Numerical results*

Energy evolution in time for the C – LES and I – LES solutions are shown in figure 4, for both LES grids. For comparison, the truncated DNS and the no-model LES solutions are also reported. The data are normalized with respect to the initial energy associated with the DNS solution truncated at $\kappa_c = 16$. It turns out that when supplying the simulation with the coherent SGS force, one obtains very good results for the energy decay (the same holds for the temporal evolution of the viscous dissipation, not reported). On the contrary, supplying the incoherent modes gives no practical contribution to the model since the I – LES solution practically coincides with the no-model one. As a trivial but necessary check, it has been verified that T – LES provides results that are indistinguishable from the filtered DNS solution. The same good behaviour of C – LES is obtained for the spectral energy distribution. For instance, energy density spectra for both grids after 10^3 time steps are illustrated in figure 5. By supplying only the incoherent SGS modes, the solution shows the same energy pile-up characteristic of the no-model solution.

Figure 6 shows the time evolution for the SGS dissipation, ϵ_{SGS}, for C – LES, I – LES and T – LES solutions. The SGS dissipation is normalized with respect to the initial viscous dissipation corresponding to the truncated DNS at $\kappa_c = 16$. It is evident how few coherent SGS modes are responsible for the right subgrid-scale energy transfer. For the coarser LES grid, trivially the SGS dissipation is more important, while the agreement between C – LES and T – LES is almost perfect. The picture is even clearer when looking at the different contributions to the SGS dissipation, $\epsilon_{SGS}^{(coh)}$ and $\epsilon_{SGS}^{(inc)}$, for the T – LES solution, plotted in figure 7. The SGS dissipation mostly comes from the coherent component, with the effect of the incoherent subgrid scales being essentially non-dissipative. In fact, a very large fraction of the SGS dissipation results
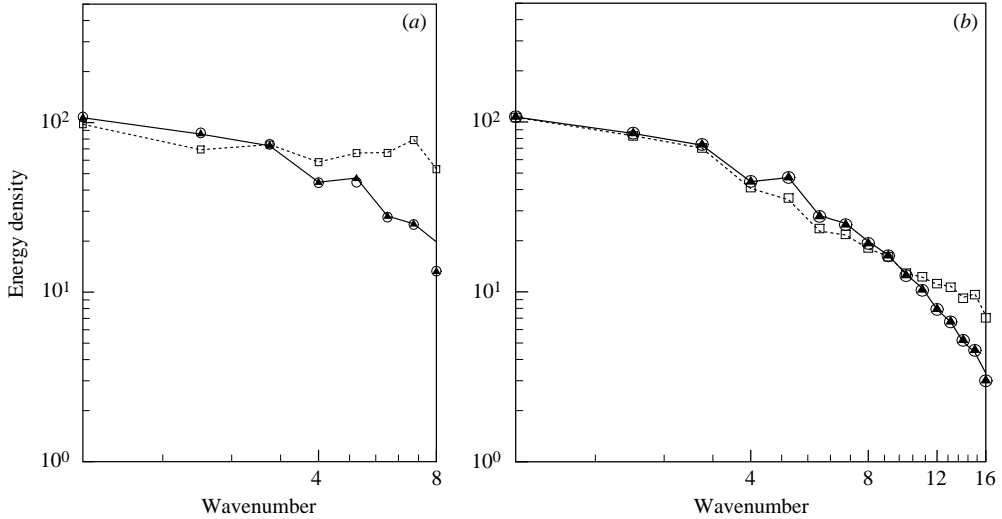
FIGURE 5. Energy spectra for C – LES (▲), I – LES (□) and B – LES (○), compared to truncated DNS (———) and no-modelled solutions (········) with (a) $\kappa_c = 8$ and (b) 16.
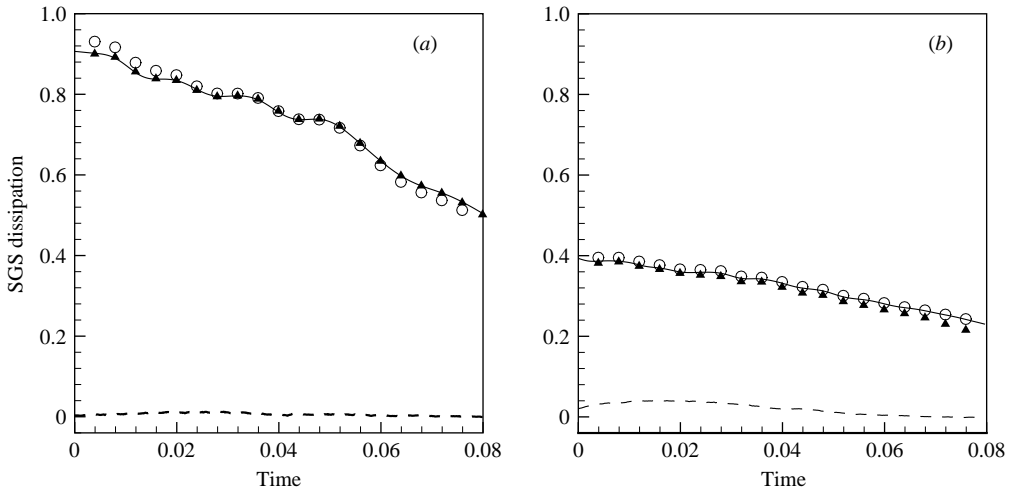

FIGURE 6. SGS dissipation for C – LES (▲), I – LES (- - -), B – LES (○) and T – LES (———) solutions with (a) $\kappa_c = 8$ and (b) 16.

from the 6% (on average) of the SGS modes that are coherent. For the smaller cutoff, coherent and total SGS dissipation are practically indistinguishable.

Note that the coherent modes must be distinguished from the 'near-band' SGS modes (Kraichnan 1976; Domaradzki *et al.* 1993, 1994), even though both coherent and 'near-band' modes contain most of the SGS energy and dominate the SGS energy transfer. In order to clearly show the distinction between these two types of modes, the dynamic tests using perfect modelling approach were conducted for LES supplied with the SGS stresses from 'near-band' modes. These results, denoted as B – LES, are also shown in figures 4–6. These figures confirm previous findings from static studies that the SGS dissipation results almost exclusively from the interactions between resolved scales and 'near-band' SGS modes. However, the fact that most of the energy in the SGS field is concentrated in the 'near-band' modes is simply a reflection of the rapid decay in the energy spectrum. Furthermore, only 3% of these 'near-band' modes are
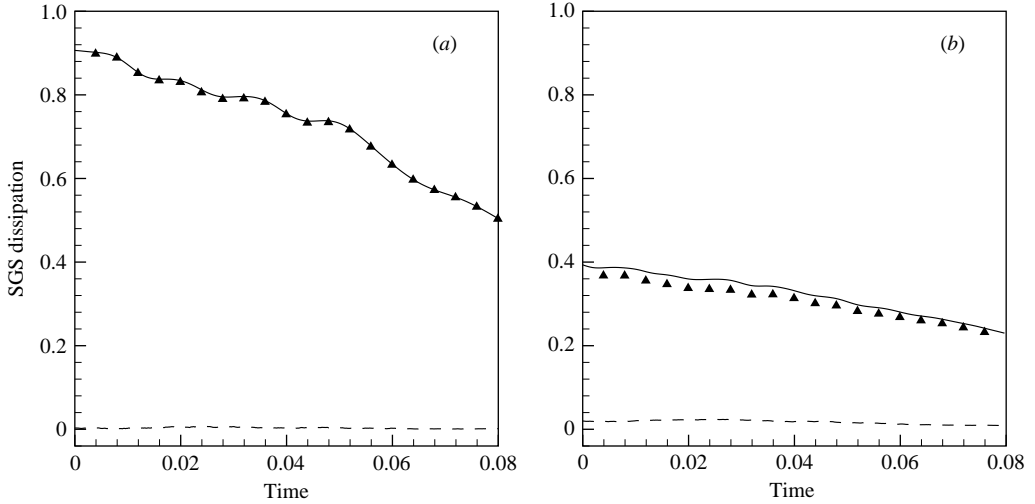
FIGURE 7. Coherent (▲) and incoherent (- - -) SGS dissipation, compared to the total one (———), for T – LES solution with (a) $\kappa_c = 8$ and (b) 16.
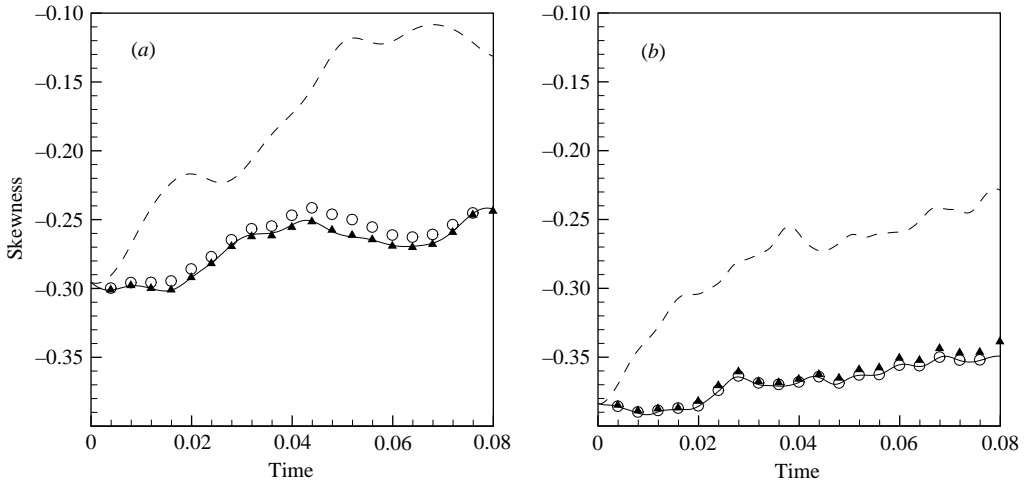

FIGURE 8. Skewness of a velocity component derivative for C – LES (▲), I – LES (- - -), B – LES (○) and T – LES (———) solutions with (a) $\kappa_c = 8$ and (b) 16.

coherent. In fact, additional LES simulations supplied with the SGS stresses only from coherent 'near-band' modes produce virtually indistinguishable results when compared to B – LES simulations. For the clarity of figures the results of these simulations are not shown. Thus, 97% of the incoherent 'near-band' modes have practically no effect on the energy transfer mechanism. This fact was overlooked by previous investigators, mostly due to the absence of a robust and efficient tool that is capable of decomposing the field into coherent and incoherent contributions. In order to see the difference between the effects of coherent and 'near-band' SGS modes, one must look at higher-order statistics. The clear differences for SGS dissipation and skewness of a velocity component derivative are observed in figure 6 and figure 8, respectively. The differences for $\kappa_c = 16$ are less pronounced, owing to the moderate Reynolds number and closeness of the cutoff wavenumber to the end of the inertial

range. It is expected that these differences would be more pronounced for higher Reynolds number flows.

4. Conclusions

The present study deals with the effect of the coherent and incoherent subgrid-scale modes in the classical LES approach. The coherent/incoherent decomposition of the SGS modes is defined using a wavelet thresholding filter, while the LES filtering, that separates the resolved LES modes from the SGS modes, is based on spectral cutoff filtering inherent in the adoption of a pseudo-spectral method for the LES simulations performed. It must be noted that this is very different from adopting the wavelet filter to separate resolved from unresolved modes, as in alternative recent approaches, such as CVS (Farge *et al.* 2001) or SCALES (Goldstein & Vasilyev 2004).

By exploiting the perfect modelling approach, it has been demonstrated that modelling incoherent SGS modes has a negligible effect upon the large-scale dynamics. Supplying pure coherent SGS stresses seems sufficient to provide results very close to cutoff-filtered (truncated) DNS data. In fact, the low-order statistics have been shown to be relatively insensitive to the effect of the incoherent SGS modes.

The strong message provided by this study is that the effect of the coherent SGS modes needs to be modelled, while modelling the incoherent stochastic component is not very important in terms of reproducing low-order statistics. This fact partially explains why deterministic SGS models work in LES, since they reproduce the effect of the coherent SGS modes on the resolved scales. The lack of success in showing significant statistical correlation in *a priori* tests may then be attributed to the dominant role of the incoherent SGS modes in any stochastic estimation.

However, further investigations are needed to assess the influence of coherent/incoherent SGS modelling on higher-order statistics. Additional tests are needed to confirm the conclusions for high Reynolds number turbulent flows. However, we believe that the conclusions drawn in this paper would hold even for high-*Re* turbulent flows, since for higher Reynolds number an even smaller percentage of coherent SGS modes is responsible for most of the global energy flux from the smallest resolved eddies to the largest unresolved ones.

REFERENCES

ADRIAN, R. 1990 Stochastic estimation of sub-grid scale motions. *Appl. Mech. Rev.* **43**, 214–218.

BARDINA, J., FERZIGER, J. H. & REYNOLDS, W. C. 1983 Improved turbulence models based on large eddy simulation of homogeneous incompressible turbulence. *Rep.* TF-19. Thermosciences Div., Dept. of Mech. Engng, Stanford University.

CANTWELL, B. 1981 Organized motion in turbulent flow. *Annu. Rev. Fluid Mech.* **13**, 457–515.

CHASNOV, J. R. 1991 Simulation of the Kolmogorov inertial subrange using an improved subgrid model. *Phys. Fluids* A **3**, 188–200.

DAUBECHIES, I. 1988 Orthonormal bases of compactly supported wavelets. *Commun. Pure Appl. Maths* **41**, 909–996.

DE STEFANO, G. & VASILYEV, O. V. 2002 Sharp cutoff versus smooth filtering in large eddy simulation. *Phys. Fluids* **14**, 362–369.

DE STEFANO, G. & VASILYEV, O. V. 2004 Perfect "modelling" framework for dynamic SGS model testing in large eddy simulation. *Theor. Comput. Fluid Dyn.* **18**, 27–41.

DOMARADZKI, J. A., LIU, W. & BRACHET, M. E. 1993 An analysis of subgrid-scale interactions in numerically simulated isotropic turbulence. *Phys. Fluids* A **5**, 1747–1759.

DOMARADZKI, J. A., LIU, W., HARTEL, C. & KLEISER, L. 1994 Energy transfer in numerically simulated wall-bounded turbulent flow. *Phys. Fluids* **6**, 1583–1599.

DONOHO, D. L. 1994 De-noising by soft-thresholding. *IEEE Trans. Inf. Theory* **41**, 613–627.

ESWARAN, V. & POPE, S. B. 1988 An examination of forcing in direct numerical simulations of turbulence. *Comput. Fluids* **16**, 257.

FARGE, M., PELLEGRINO, G. & SCHNEIDER, K. 2001 Coherent vortex extraction in 3D turbulent flows using orthogonal wavelets. *Phys. Rev. Lett.* **87**, 054501.

FARGE, M., SCHNEIDER, K. & KEVLAHAN, N. 1999 Non-Gaussianity and coherent vortex simulation for two-dimensional turbulence using an adaptive orthogonal wavelet basis. *Phys. Fluids* **11**, 2187–2201.

GERMANO, M., PIOMELLI, U., MOIN, P. & CABOT, W. 1991 A dynamic subgrid-scale eddy viscosity model. *Phys. Fluids* A **3**, 1760–1765.

GOLDSTEIN, D. A. & VASILYEV, O. V. 2004 Stochastic coherent adaptive large eddy simulation method. *Phys. Fluids* **16**, 2497–2513.

HUSSAIN, A. K. M. F. 1986 Coherent structures and turbulence. *J. Fluid Mech.* **173**, 303–356.

JIMENEZ, J., WRAY, A., SAFFMAN, P. & ROGALLO, R. 1993 The structure of intense vorticity in isotropic turbulence. *J. Fluid Mech.* **225**, 65–90.

KRAICHNAN, R. 1976 Eddy viscosity in two and three dimensions. *J. Atmos. Sci.* **33**, 1521–1536.

LANGFORD, J. & MOSER, R. D. 1999 Optimal LES formulations for isotropic turbulence. *J. Fluid Mech.* **398**, 321–346.

LEITH, C. E. 1990 Stochastic backscatter in a subgrid-scale model: Plane shear mixing layer. *Phys. Fluids* A **2**, 297–299.

LESIEUR, M. 1997 *Turbulence in Fluids*. Kluwer.

LESIEUR, M. & MÉTAIS, O. 1996 New trends in large-eddy simulations of turbulence. *Annu. Rev. Fluid Mech.* **28**, 45–82.

MALLAT, S. G. 1999 *A Wavelet Tour of Signal Processing*. Academic.

MENEVEAU, C. & KATZ, J. 2000 Scale-invariance and turbulence models for large-eddy simulation. *Annu. Rev. Fluid Mech.* **32**, 1–32.

SMAGORINSKY, J. S. 1963 General circulation experiments with the primitive equations. *Mon. Weather Rev.* **91**, 99–164.

SWELDENS, W. 1998 The lifting scheme: A construction of second generation wavelets. *SIAM J. Math. Anal.* **29**, 511–546.

VASILYEV, O. V. 2003 Solving multi-dimensional evolution problems with localized structures using second-generation wavelets. *Intl J. Comput. Fluid Dyn.,* Special issue on High-resolution methods in Computational Fluid Dynamics **17**, 151–168.

VINCENT, A. & MENEGUZZI, M. 1991 The spacial structure and statistical properties of homogeneous turbulence. *J. Fluid Mech.* **225**, 1–20.